K.P. Singh
President and CEO
Holtec International

Study of Bolted Joint Integrity and Inter-Tube-Pass Leakage in U-Tube Heat Exchangers

Part I: Analysis

"Three element bolted joints," consisting of an unstayed tubesheet sandwiched between two tapered hub flanges, find extensive use in U-tube type heat exchangers. A comprehensive analysis technique is herein developed to investigate the structural characteristics of such joints. Design strategies to reduce stress levels in the tubesheet and the flanges are proposed. In particular, the concept of "controlled" metal-to-metal contact beyond the bolt circle between the mating surfaces is introduced and explored in depth. The solution is readily programmed on a digital computer for application in analysis oriented design evaluation and optimization studies.

1 Introduction

From a structural viewpoint, the bolted joint is perhaps the most vulnerable region in a heat exchanger. Whereas few pressure vessels are known to fail by elastic buckling, bursting, or plastic collapse, "leaky" joints are not too infrequent. This fact was not lost on the researchers in the early stages of the inception of pressure vessel technology, as is evidenced by the number of significant contributions on this subject in that period [1].[1] Of numerous excellent articles on this problem, special mention is due to the work by Waters, et al. [2] which gave the general basis for the design rules in the ASME Code [3]. In their bid to develop design rules of manageable numerical tedium, Waters, et al., assume that the bolt stress does not change due to pressurization of the joint. Thus, in essence, the stress in bolts under the operating conditions cannot be determined by this method, even as the ASME Code [3, p. 328] prescribes a limit on the "service stresses." Evaluation of the service stresses is important to determine the fatigue life of bolts in bolted joints subject to pulsating operating pressures.

In this work, our principal object is to accurately characterize the behavior of bolted joints as they occur in tubular heat exchangers. For purposes of illustrating the basic concepts developed here, a common bolted joint used in removable bundle U-tube type heat exchangers is considered. As shown in Fig. 1, in this construction, the tubesheet is sandwiched between two tapered hub flanges (also called "welding neck flanges"). Thus, the bolted joint consists of three elements, namely two flanges and the tubesheet. A formalism to define the structural response of the bolted joint is developed herein which can be utilized to evaluate the design concepts aimed to maintain joint sealability. Furthermore, this analysis enables an in-depth study of other important joint characteristics; e.g., bolt stress variations with operating pressure pulsations, gasket hysteresis, etc.

Another object of this paper is to develop a solution technique to evaluate the effect of metal-to-metal contact on the joint response. Metal-to-metal contact (henceforth abbreviated as MTM) at the outer edges of the mating members may be effected during the seating condition by suitably machining the flange faces. Even an edge contact load under the seating condition may be induced. Or a certain edge gap may be prescribed under the seating condition which diminishes to zero and further develops an edge contact load as the internal joint pressure is applied. This latter case may be labeled as "controlled" MTM condition.

The third objective of this paper is to develop the solution technique to evaluate the stress fields in the tubesheet and the two flanges.

A major motivation for this analysis follows from considerations of functional performance of U-tube heat exchangers. An improperly

[1] Numbers in brackets designate References at end of paper.

Contributed by the Nuclear Engineering Division and presented at the Winter Annual Meeting, Atlanta, Ga., November 27–December 2, 1977 of THE AMERICAN SOCIETY OF MECHANICAL ENGINEERS. Manuscript received at ASME Headquarters August 3, 1977. Paper No. 77-WA/NE-6.

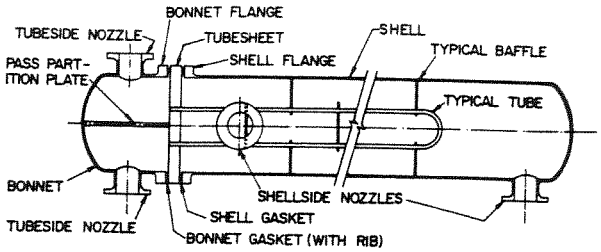

Fig. 1 A two tube pass removable bonnet heat exchanger

designed bolted joint may exert insufficient edge restraint on the tubesheet (Fig. 1) during the operating condition. In those applications where the tubeside operating pressure is substantially higher than the shellside operating pressure, the lateral deflection of the tubesheet can develop a narrow crevice between the tubesheet and the pass partition plates. This gap, although small in width, can cause a measurable fraction of the tubeside fluid to "short circuit" between the tube passes, and thus significantly derate the heat exchanger. Further discussion of this problem may be found in a sequel to this paper [16].

In a notable work on tubesheets for U-tube heat exchangers, Gardner [6] gives a complete method for designing the tubesheets, taking into account the rotational resistance offered by the tubes. Inclusion of this effect implies that the baffle holes in the baffles adjacent to the tubesheet are drilled to a minimum tolerance. This assumption may be realized in a well controlled fabrication process. However, due to the delicate nature of this assumption, we do not take credit for the tubes, although the ASME appears to be proceeding to incorporate it in a future edition of their pressure vessel codes [5]. Other major assumptions are:

1 The strengthening effects of the pass partition lanes in the tubesheet and pass partition plates in the bonnet flange are ignored.

2 The untubed region and the flanged portion of the tubesheet are modeled as a ring, rather than a plate. Similarly, the flange rings are treated by "ring theory" rather than "plate theory".

3 The weakening effect of the bolt holes in the flanges and the tubesheet is neglected.

Foregoing assumptions 2 and 3 can be eliminated without conceptually altering the method of analysis. However, they are introduced here to simplify the treatment.

In the interest of clarity, it is perhaps most logical to first derive the equations for the structural response of the tubesheet and the flanges, and then describe the solution procedure to determine the bolt stress, flange and tubesheet stress fields and other quantities of interest.

The solution technique described here is applied to a typical practical example problem in a sequel to this paper [16], wherein an algorithm to estimate the effect of bolted joint characteristics on heat transfer performance is also devised.

2 The Structural Model

Fig. 2 shows the mathematical model of the bolted joint. The tubesheet is sandwiched between two flanges, which are henceforth referred to as the "Channel (Bonnet) Flange" and "Shell Flange," respectively. We will refer to this assembly as a "three element joint" in our further discussions. The bolts pass through clearance holes in

Nomenclature

a = tubesheet interface radius
a_i' = mean radius (i = 1, channel; i = 2, shell)
A_b = root area of body bolts
a^* = mean radius of tubesheet rim
b_i' = width of channel (i = 1), and shell flange (i = 2) rings
B' = bolt load per unit circumference (Fig. 2)
b = outer radius of the tubesheet and flanges
c = radial distance between bolt center line and gasket reaction line
D_i = flexural rigidity of channel (i = 1), and shell (i = 2)
d_i = radial distance between bolt center line and hub center line at large end (i = 1, channel flange; i = 2, shell flange)
E_1 = equivalent Young's modulus of perforated tubesheet region
E_2 = Young's modulus of tubesheet material
E_i' = Young's modulus of channel (i = 1), and shell material (i = 2)
f_i = flange thickness (i = 1, channel; i = 2, shell)
F_1 = channel gasket surface pressure resultant
F_2 = shell gasket surface pressure resultant
F_e = edge contact load per unit circumference between channel flange and tubesheet
h_p = ligament width
h = width of tubesheet untubed rim
K = joint stiffness (equation (44))
K_b = bolt stiffness (equation (46))
k' = stress multiplier (equation (18.b))
ℓ_0 = bolt length under prestress (unpressurized condition)
m = gasket factor (defined in reference [3, p. 291])
M_0 = radial bending moment at tubesheet interface radius a
Mr_{max} = maximum radial bending moment in tubesheet
M_{1i}, M_{2i} = bending moment per unit circumference at the shell-hub and hub-ring junction, respectively (i = 1 channel, i = 2, shell)
M_h = maximum longitudinal moment in the flange hub
n = number of bolts
P = tube pitch
p_1 = channel side pressure
p_2 = shell side pressure
Q_0 = shear force per unit circumference at the interface between the rim and the perforated interior
Q_{1i}, Q_{2i} = shear force per unit circumference at the hub-shell and hub-ring junctions, respectively (i = 1 channel flange, i = 2 shell flange)
r_{max} = radius of the outermost tube hole center in the tubesheet
r_1 = effective channel gasket radius
r_2 = effective shell gasket radius
r_b = bolt circle radius
r_1' = mean radius of channel (i = 1) and shell flange rings (i = 2)
s = term representing the cumulative contribution of machining of the bolted joint elements
t_i = thickness of channel (i = 1) or shell (i = 2)
t_s = thickness of the tubesheet
$w(r)$ = deflection of tubesheet with respect to $r = r_1$ (point B in Fig. 3)
x_1, x_2 = distance of small and large end of the hub from the point of zero thickness (Fig. 4)
y = ASME code gasket seating stress
α = slope of flange hub
δ_i = thickness of gasket (i = 1 channel side, i = 2 shell side)
$\delta(r)$ = thickness of channel gasket rib at radius r
ϵ_0 = initial edge gap
ϵ_1 = edge gap between channel flange and tubesheet under pressurized condition
$\zeta(r)$ = gap at radius r
η = ligament efficiency
θ_i = rotation of channel flange ring (i = 1), and shell flange ring (i = 2), respectively
θ_s = rotation of tubesheet rim
ν_1 = Poisson's ratio of perforated tubesheet region
ν_2 = Poisson's ratio of tubesheet material
ν_i' = Poisson's ratio of shell and channel materials, respectively (i = 1, 2)
σ_0 = prestress (seating stress) in bolts
σ = service bolt stress
σ_t = maximum bending stress in the perforated plate
σ_r = flange ring bending stress

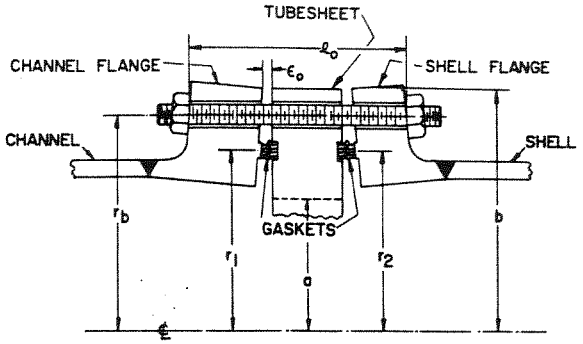

Fig. 2 Bolted joint under seating condition

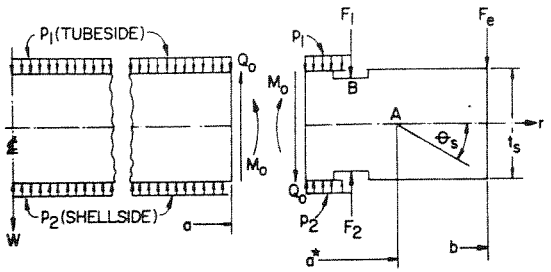

Fig. 3 Freebody of the tubesheet

the tubesheet. We assume that there are n bolts of root area A_b prestressed to a certain known stress level, σ_0. It is further assumed that the channel flange bears against the gasket on the tubesheet groove, and it may have an initial edge gap ϵ_0 under the "seating condition," [2] or it may develop an edge contact load F_e per unit circumference. The edge gap ϵ_0 or edge contact load F_e are design options which can be easily adjusted in a joint assembly by properly machining the flange/tubesheet surface. The shell flange, however, is assumed to bear totally against the gasket, i.e., it does not make metal-to-metal contact either during the seating or the pressurized condition. This assumption is not a limitation of the mathematical analysis. Rather, it is guided by certain design considerations which are described fully in a later section.

The mathematical model for the gasket presents the greatest problem. A typical spiral wound gasket possesses highly nonlinear and nonconservative loading, unloading and reloading characteristics [7]. Furthermore, the minimum surface pressure on the gasket to maintain a leak-tight joint depends on a host of parameters, such as surface finish, groove clearance, gasket strip material, filler material, loading history, properties, etc. Strictly speaking, if the stress-strain relationship of the gasket is known, then the "exact" pressure distribution on the gasket can be determined as a function of the rotation of the mating surfaces. Since the rotation of the mating flanges themselves will depend on the gasket surface pressure distribution, an iterative solution will have to be devised. In reality, however, precise data on the gasket stiffness characteristics are seldom available. Hence, in most cases, improvement in the results by making an accurate mathematical model of the gasket will not be realized. In view of this, a simplified model for the gasket is assumed here. We borrow the assumption of the ASME Code [3] that the gasket pressure resultant acts at the "effective gasket diameter," irrespective of the flange rotations. However, the loading and unloading stiffnesses are allowed to be an arbitrary (known) function of the compression and decompression history.

We next proceed to set up the governing equations for the structural response of the tubesheet and flange cross sections.

3 Tubesheet

The tubesheet contains a perforated interior in which the tube holes are arranged in a geometric pattern on a specified pitch, P. Following the ASME Code [3, p. 431], the outer radius of the perforated interior may be defined as

$$a = r_{\max} + \frac{P - h_p}{4} \tag{1a}$$

where $r_{\max}$ is the radius of the outermost tube center, and h_p is the ligament width. The ligament efficiency, η, of the perforations is defined as

$$\eta = \frac{h_p}{P} \tag{1b}$$

[2] Used in reference [3] to indicate the condition of bolt prestress.

It is well known [8–10] that the perforated region may be idealized as a homogeneous, isotropic plate of modified elastic constants. The modified elastic constants are given as function of η, and the elastic constants of the plate material for any given tube layout pattern. Thus, the tubesheet is modeled as a composite plate consisting of two concentric circular plates bonded at the interface radius a.

The outer plate is modeled as an elastic ring. In Fig. 3, F_1 and F_2 denote the tubeside and shellside gasket reaction resultants, respectively. F_e denotes the edge contact load between the channel flange and the tubesheet. p_1 and p_2 are tubeside and shellside pressures, assumed to act up to radii r_1 and r_2, respectively, where r_1 and r_2 are the effective gasket radii. Thus, the mean radius of the rim (point A in Fig. 3) is given by

$$a^* = 0.5(a + b) \tag{2}$$

and the width of the ring, h is given by

$$h = (b - a) \tag{3}$$

Let;

$$p = p_1 - p_2 \tag{4}$$

Then the shear force Q_0 at the rim-perforated plate interface follows from equilibrium:

$$Q_0 = \frac{pa}{2} \tag{5}$$

Furthermore, the net moment about point A is given by

$$M = M_0 - \frac{Q_0 h}{2} - F_1(a^* - r_1) + F_e(b - a^*) - \frac{p_1(r_1 - a)(2a^* - r_1 - a)}{2} + F_2(a^* - r_2) + \frac{p_2(r_2 - a)(2a^* - r_2 - a)}{2} \tag{6}$$

Thus

$$M = M_0 - \chi \tag{7}$$

where

$$\chi = \frac{pah}{4} + F_1(a^* - r_1) - F_2(a^* - r_2) - F_e(b - a^*) + \frac{p_1(r_1 - a)(2a^* - r_1 - a)}{2} - \frac{p_2(r_2 - a)(2a^* - r_2 - a)}{2} \tag{8}$$

The rotation of the rim, θ_s, due to M follows from elementary strength of materials theory.

$$\theta_s = \frac{12a^{*2}(M_0 - \chi)}{E_2 h t_s^3} \tag{9}$$

We will next set up the governing equations for the perforated interior modeled as an equivalent solid plate in the manner described before. The governing differential equation for axisymmetric de-

flection of circular plates is well known [11]

$$\left(\frac{d^2}{dr^2}+\frac{1}{r}\frac{d}{dr}\right)\left(\frac{d^2}{dr^2}+\frac{1}{r}\frac{d}{dr}\right)w=\frac{p}{D_1} \tag{10}$$

where the plate flexural rigidity is defined as

$$D_1=\frac{E_1 t_s{}^3}{12(1-\nu_1{}^2)} \tag{11}$$

The general solution of equation (10) is given by

$$w=\gamma_1+\gamma_2 r^2+\gamma_3\,\ell n\, r+\gamma_4 r^2\,\ell n\, r+\frac{Pr^4}{64D_1} \tag{12}$$

where $\gamma_i (i = 1, 4)$ are arbitrary constants of integration. For a solid plate (no hole in the center) finiteness of deflection and slope at $r = 0$ yield $\gamma_3 = \gamma_4 = 0$. γ_1 and γ_2 are determined by the boundary conditions. By appealing to continuity of slope, and traction (radial moment) at $r = a$, and performing the necessary algebra, the following results are derived.

$$\gamma_2=\frac{6a^{*2}(M_0-\chi)}{E_2 h a t_s{}^3}-\frac{pa^2}{32D_1} \tag{13}$$

$$M_0=\frac{1}{1+\rho}\left(\rho\chi-\frac{pa^2}{8}\right) \tag{14}$$

where

$$\rho=\frac{12a^{*2}D_1(1+\nu_1)}{E_2 h a t_s{}^3} \tag{15}$$

The deflection of the tubesheet with respect to the rim is given by

$$w^*=\gamma_2(r^2-a^2)+\frac{p}{64D_1}(r^4-a^4) \tag{16}$$

Thus, the deflection of the tubesheet at a radius r with respect to point B $(r = r_1)$ is given by

$$\begin{aligned} w &= -(r_1-a)\theta_s+w^* \qquad r\le a \\ &= -(r_1-r)\theta_s \qquad r\ge a \end{aligned} \tag{17}$$

The radial bending moment M_r is given by

$$M_r=-2\gamma_2 D_1(1+\nu_1)-\frac{(3+\nu_1)pr^2}{16}; \qquad r\le a \tag{18a}$$

The maximum bending stress in the perforated plate averaged across the ligament width is given by [3, p. 435]

$$\sigma_t=\frac{k'}{\eta}\frac{6M}{t_s{}^2} \tag{18b}$$

where k' is the "stress multiplier" given in reference [3] as a function of the stress ratio; and M is the larger of the radial and circumferential bending moments. ASME design rules limit σ_t to 150 percent of the allowable stress in the tubesheet material at the design temperature.

4 Flange

The flange may be viewed as a structural member consisting of a ring and a tapered hub butt welded to the cylindrical shell. Conceptually, the operation of a tapered hub flange is quite simple. As shown in Fig. 4, the gasket is compressed to a desired value by prestressing the bolts. The tensile force in the bolts, and the surface compression on the gasket constitute a couple which produces rotation in the flange ring and a state of stress in the flange. When pressure is applied, the hydrostatic end force, W, in the shell in general produces additional rotation of the flange ring, and elongation (or contraction) of the bolt. The surface pressure on the gasket is reduced, and the stress field in the flange is altered. One basic objective in the flange design is to ensure that the stress levels in the flange do not exceed postulated allowables. The flange design methods given in the ASME Codes [3], and several others, base the design criteria strictly on the stress limits. Arguably, the stress limit based design methods

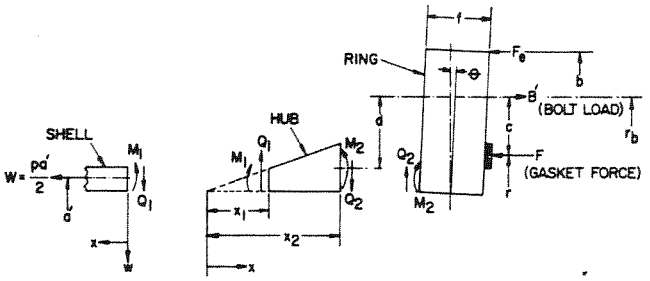

Fig. 4 Flange stress analysis model

do not offer any assurance of sealability; they merely protect the flange from gross plastic deformations. A more direct measure of sealworthiness of a pressurized bolted joint lies in the magnitude of the residual pressure on the gasket. The magnitude of this residual pressure depends on numerous factors, such as flange ring rotation, bolt stretch (or contraction), gasket stress-deformation characteristics, flange geometry, the structural characteristics of the mating member, etc. The mathematical complexity attendant to the calculation of the residual pressure has presumably precluded its use as a design criterion. However, a complete analysis of the bolted joint structural response requires evaluation of the gasket residual pressure, flange stress field and bolt stress variation. Fittingly, this subject has commanded the attention of numerous investigators. Reference [13] contains an excellent synopsis and bibliography of many research papers on this topic. Of these, the solution of Murray and Stuart [12] appears to be the most adaptable to our needs. Murray and Stuart [12] appeal to the classical shell and ring theories to set up an 8×8 linear equation set which can be solved to determine the discontinuity moments and shear forces at the hub-shell and hub-ring junctions. The elastic behavior of the tapered hub is described by the formulation given in reference [11, p. 488].

This analysis has two main limitations, namely;

1 The flange ring is treated by ring theory rather than plate theory.

2 The mean diameter of the hub and the shell are taken equal to the mean shell diameter.

These limitations, although important from a purely mathematical viewpoint, are of minor importance for commercial units of moderate sizes (e.g., over 20″ diameter). The solution of Murray and Stuart is extended and modified here. The important steps and results are abstracted in the following for the sake of completeness and readability. The solution given below applies to both shell and channel flanges. We will use symbols for the generic variables without subscripts in this section. In later sections, wherever a distinction is necessary, subscripts 1 and 2 are appended to the variables to indicate the quantities pertaining to the channel and shell flanges, respectively. Referring to Fig. 4, the radial displacement w of the shell (positive if directed towards the center) is given in terms of the edge shear Q_1, and moment M_1, as [11, p. 469],

$$w=\frac{e^{-\beta x}}{2\beta^3 D}\left[\beta M_1(\sin\beta x-\cos\beta x)+Q_1\cos\beta x\right]-\frac{pa'^2}{E't}(1-0.5\nu) \tag{19}$$

where

$$\beta=\left[\frac{3(1-\nu'^2)}{a'^2 t^2}\right]^{1/4} \tag{20}$$

and

$$D'=\frac{E't^3}{12(1-\nu'^2)} \tag{21}$$

The radial displacement w of the tapered hub is expressed in terms of the longitudinal coordinate measured from the point of zero

thickness. Thus, the thickness of the hub at the small end (equal to the shell thickness) is

$$t = \alpha x_1 \tag{22}$$

where α is the rate of taper. We have

$$w = x^{-1/2}[c_1\psi_1'(\epsilon) + c_2\psi_2'(\epsilon) + c_3\psi_3'(\epsilon) + c_4\psi_4'(\epsilon)] - \frac{pa^2}{E\alpha x}\left(1 - \frac{\nu'}{2}\right) \tag{23}$$

where

$$\epsilon = 2\rho\, x^{1/2} \tag{24}$$

and

$$\rho = \left[\frac{12(1-\nu'^2)}{\alpha^2 a'^2}\right]^{1/4} \tag{25}$$

$c_i (i = 1\text{–}4)$ are constants of integration and the ψ's are the so called Schleicher functions, akin to the well known Kelvin functions. The series expansion of these functions is given in the Appendix. The bending moment M_x and shear force Q_x follow by successive differentiations of equation (23). We have

$$Q_x = \frac{E'\alpha^3\rho^2 x^{1/2}}{24(1-\nu'^2)}[c_1S_2(\epsilon) + c_2S_1(\epsilon) + c_3S_4(\epsilon) + c_4S_3(\epsilon)] \tag{26}$$

$$M_x = \frac{E'\alpha^3 x^{1/2}}{48(1-\nu'^2)}[c_1S_5(\epsilon) - c_2S_6(\epsilon) + c_3S_7(\epsilon) - c_4S_8(\epsilon)] + \frac{pa^2\alpha^2}{6(1-\nu'^2)}(1 - 0.5\nu') \tag{27}$$

The functions $S_i(\epsilon)$ are combinations of Schleicher functions and their derivatives. These are defined in the Appendix. Force equilibrium yields

$$r_bB' - bF_e - rF - \frac{pr^2}{2} = 0 \tag{28}$$

where B', F_e, and F are bolt load, edge force (zero for shell flange) and gasket load per unit circumference. The rotation of the flange ring, θ, is given by

$$\theta = \frac{12r'^2M}{E'b'f^3} \tag{29}$$

where the applied moment M is given by

$$M = M_2 + \frac{Q_2 f}{2} + \Lambda \tag{30}$$

where

$$\Lambda = -\frac{F_e b(r - r_b)}{r_b} + \frac{Fr}{r_b}(r_b - r) + \frac{pa'^2d}{2r_b} + \frac{p(r^2 - a'^2)(2r_b - r - a)}{4r_b} \tag{31}$$

Finally, the radial displacement of the ring at its junction with the hub is given by:

$$w = -\left(p + \frac{Q_2}{f}\right)\frac{r'^2}{b'E'} - \frac{6r'^2M}{E'b'f^2} \tag{32}$$

By matching the displacement, slope, shear force and bending moment at the two locations of discontinuity, eight linear algebraic equations are obtained, which may be written in subscript notation as

$$m_{ij}c_j = n_i;\ i, j = 1, 2, \ldots 8. \tag{33}$$

The unknown vector c_j consists of the four constants of integration in equation (23), and four discontinuity reactions with the notation,

$$c_5 = M_1,\ c_6 = Q_1,\ c_7 = M_2,\ c_8 = Q_2$$

The nonzero elements of m_{ij} and n_i are defined as follows:

$$m_{(2i-1)j} = \frac{2\rho}{\epsilon_i}\psi_j'(\epsilon_i); \qquad \begin{matrix} i = 1, 2 \\ j = 1, 2, 3, 4 \end{matrix}$$

where

$$\epsilon_i = 2\rho x_i^{1/2}; \qquad i = 1, 2$$

x_1 and x_2 are shown in Fig. 4 (hub end coordinates)

$$m_{15} = \frac{1}{2\beta^2D'}; \qquad m_{16} = -\frac{1}{2\beta^3D'}$$

$$m_{2i,j} = (-1)^{j+1}\frac{4\rho^3}{\epsilon_i^3}S_j(\epsilon_i); \qquad \begin{matrix} i = 1, 2 \\ j = 1, 2, 3, 4 \end{matrix}$$

$$m_{25} = \frac{1}{\beta D'}; \qquad m_{26} = -m_{15}$$

$$m_{37} = \frac{6r'^2}{E'b'f^2}; \qquad m_{38} = \frac{4r'^2}{E'b'f}$$

$$m_{47} = -\frac{12r'^2}{E'b'f^3}; \qquad m_{48} = -\frac{6r'^2}{E'b'f^2}$$

$$m_{3+2i,j} = (-1)^{j+1}S_{4+j}(\epsilon_i); \qquad \begin{matrix} i = 1, 2 \\ j = 1, 2, 3, 4 \end{matrix}$$

$$m_{55} = \frac{96\rho(1-\nu'^2)}{E'\alpha^3\epsilon_1}$$

$$m_{4+2i,j} = S_{j+1}(\epsilon_i); \qquad i = 1, 2; \qquad j = 1, 3$$

$$m_{4+2i,j} = S_{j-1}(\epsilon_i); \qquad i = 1, 2; \qquad j = 2, 4$$

$$m_{66} = \frac{-48(1-\nu'^2)}{E'\alpha^3\rho\epsilon_1}; \qquad m_{77} = \frac{96\rho(1-\nu'^2)}{E'\alpha^3\epsilon_2}$$

$$m_{88} = \frac{-48(1-\nu'^2)}{E'\alpha^3\rho\epsilon_2}; \qquad n_2 = \frac{pa'^2(1-0.5\nu')}{E'\alpha x_1^2}$$

$$n_3 = \frac{pa'^2(1-0.5\nu')}{E'\alpha x_1} - \frac{pr'^2}{b'E'} - \frac{6r'^2\Lambda}{E'b'f^2}$$

$$n_4 = \frac{-pa'^2(1-0.5\nu')}{E'\alpha x_2^2} + \frac{12r'^2\Lambda}{E'b'f^3}$$

$$n_{3+2i} = \frac{16pa'^2\rho(1-0.5\nu')}{E'\alpha\epsilon_i}; \qquad i = 1, 2$$

Equation (33) can be solved to determine the stress and displacement field in the flange for any given edge load F_e, pressure p and bolt load B'. The main weakness in the above formulation lies in the modeling of the tapered hub as a cylindrical shell of variable thickness. The moment due to the hydrostatic end load in the shell, W, is assumed to act at the ring-hub junction along the midpoint of the hub. This, as described in reference [13], amounts to neglecting a moment equal to $W\alpha(x_2 - x_1)/2$. However, the error is too small in most practical cases to warrant any further refinement.

5 Method of Solution

The physical dimensions of the bolted joint and its elements are assumed to be known. The bolts, n in number of root area A_b each, are assumed to be prestressed to a desired value σ_0. The object is to determine the service bolt stress σ, maximum hub and ring stresses in the bonnet and shell flanges, maximum stress in the tubesheet, and finally, the leakage areas formed by the deflection of the tubesheet and the bonnet flange when the channel and shell chambers are subjected to pressures p_1 and p_2, respectively. Within the framework of the available data, two design parameters can be varied, namely the prestress σ_0, and the "initial edge gap" ϵ_0, between the outer edges of the bonnet flange and the tubesheet under the seating condition. ϵ_0 can be varied by properly machining the faces of the bonnet flange and/or the tubesheet beyond the gasket seating surface. We will examine the influence of these parameters on the aforementioned quantities of interest.

The force equilibrium for the bonnet flange yields the linear gasket force F_1^0 on the bonnet gasket,

$$F_1^0 = \frac{n\sigma_0 A_b}{2\pi r_1} - \frac{bF_e^0}{r_1} \tag{34}$$

where F_e^0 is the initial edge contact force per unit circumference. Note $F_e^0 = 0$ if $\epsilon_0 > 0$. Equation (34) determines the linear force on the bonnet gasket. Let δ_i^0 represent the compressed thickness of the gasket under F_1^0. Similarly the linear compression force F_2^0 on the shell gasket follows from force equilibrium:

$$F_2^0 = \frac{n\sigma_0 A_b}{2\pi r_2} \tag{35}$$

The corresponding gasket thickness is given by δ_2^0.

Using the method described in the preceding sections, the rotations of the bonnet flange θ_1^0, shell flange θ_2^0, and tubesheet θ_s can be determined, i.e.,

$$\theta_1^0 = \xi_1(F_1^0, \sigma_0, F_e^0)$$
$$\theta_2^0 = \xi_2(F_2^0, \sigma_0)$$
$$\theta_s^0 = \xi_s(F_1^0, F_2^0, F_e^0) \tag{36}$$

The superscript 0 is appended to the quantities to indicate that these pertain to the seating condition. Thus the effective bolt length under the prestress condition, ℓ_0 (Fig. 2) is given by

$$\ell_0 = s + f_1 \sec\theta_1^0 + \text{iff}_2 \sec\theta_2^0) + t_s \sec\theta_s^0 - (r_b - r_1) \times \sin\theta_1^0 - (r_b - r_2)\sin\theta_2^0 + (r_2 - r_1)\sin\theta_s^0 + \delta_1^0 + \delta_2^0 \tag{37}$$

For small values of θ_1^0, θ_2^0 and θ_s^0, equation (37) can be further simplified

$$\ell_0 = s + f_1 + f_2 + t_s + \delta_1^0 + \delta_2^0 - (r_b - r_1)\theta_1^0 + (r_2 - r_1)\theta_s^0 - (r_b - r_2)\theta_2^0 \tag{38}$$

where the term s represents the total effect of the difference between the joint thickness at the bolt center line and that at the gasket locations.

Equation (38) defines the quantity ℓ_0. We further note that the edge gap ϵ_0 is given by

$$\epsilon_0 = s_1 + \delta_1^0 - (b - r_1)(\theta_1^0 - \theta_s^0) \tag{39}$$

where s_1 represents the term due to the face machining of the mating elements. As stated before, ϵ_0 can be set equal to a small positive quantity (by adjusting s_1). Further, ϵ_0 can be zero, and an initial edge contact load F_e^0 may be developed on the channel flange-tubesheet outer edge. In short, the initial condition at the outer edge can be suitably prescribed. Our object now is to investigate the behavior of the flanged joint and its constituent elements when the two chambers are pressurized. If σ and F_e denote the "correct" bolt stress and edge load respectively, under this condition, then the channel gasket residual linear force F_1 follows from force equilibrium (equation (28))

$$F_1 = \frac{n\sigma A_b}{2\pi r_1} - \frac{bF_e}{r_1} - \frac{p_1 r_1}{2} \tag{40}$$

Similarly, the residual linear force F_2 on the shell gasket is given by

$$F_2 = \frac{n\sigma A_b}{2\pi r_2} - \frac{p_2 r_2}{2} \tag{41}$$

Let δ_1 and δ_2 denote the channel and shell gasket thicknesses corresponding to F_1 and F_2, respectively. The magnitudes of δ_1 and δ_2 depend on the gasket stiffness characteristics, as described in section 2.

The solution procedure to determine σ, F_e, and other field quantities, consists of two steps which may be stated as follows:

Step I. It is assumed *a'*-priori that there is no edge contact under the pressurized condition; i.e., $\epsilon_1 > 0$, and $F_e = 0$. The appropriate bolt stress σ, *under this assumption*, is calculated iteratively as follows.

(*a*) Assume $\sigma = \sigma_0$, evaluate F_1 and F_2 using equations (40) and (41), respectively ($F_e = 0$ in equation (40)).

(*b*) Compute bonnet flange ring rotation θ_1, shell flange ring rotation θ_2, and tubesheet rotation θ_s (equation (36)), i.e.,

$$\theta_1 = \xi_1(F_{1,\sigma})$$
$$\theta_2 = \xi_2(F_{2,\sigma})$$
$$\theta_s = \xi_s(F_1, F_2) \tag{42}$$

(*c*) Evaluate δ_1 and δ_2 corresponding to F_1 and F_2 using the gasket loading-unloading diagram.

(*d*) The effective length of the bolt ℓ under this condition is given by equation (38).

$$\ell = s + f_1 + f_2 + t_s + \delta_1 + \delta_2 - (r_b - r_1)\theta_1 + (r_2 - r_1)\theta_s - (r_b - r_2)\theta_2 \tag{43}$$

(*e*) Assume another value of σ (close to the value assumed in (*a*)), say σ'; and following the steps (*a*) through (*d*), compute the corresponding bolt length ℓ'.

(*f*) The joint stiffness K is then defined as

$$K = \frac{\sigma - \sigma'}{\ell - \ell'} \tag{44}$$

(*g*) The corrected bolt length $\ell_c = (\ell_0 + \lambda)$ is then defined by

$$\lambda = \frac{K(\ell_0 - \ell) + \sigma - \sigma_0}{K_b - K} \tag{45}$$

where bolt stiffness K_b is defined by

$$K_b = \frac{E_b}{\ell_0} \tag{46}$$

Thus the corrected bolt stress, σ_c is given by

$$\sigma_c = \sigma_0 + K_b \cdot \lambda \tag{47}$$

If the gaskets behave as (or are modeled as) linear springs, then equation (47) gives the correct bolt stress. If, however, the gasket load-deflection relationship is nonlinear, then further iteration is necessary. In the latter case, σ is set equal to σ_c in the foregoing step (*a*), and the procedure is repeated. Convergence is obtained when the assumed bolt stress σ (step *a*) equals the corrected stress σ_c (step *g*) within a prescribed tolerance.

Having determined the correct bolt stress, σ, the remaining quantities of interest, such as θ_1, θ_2, and θ_s, follow from equation (42).

The edge gap ϵ_1 under the service condition can now be determined.

$$\epsilon_1 = \epsilon_0 + \delta_1 - \delta_1^0 - (b - r_1)(\theta_1 - \theta_s - \theta_1^0 + \theta_s^0) \tag{48}$$

If $\epsilon_1 > 0$, then the assumption for zero edge load made in the beginning is verified, and the results obtained above are established to be correct. However, if $\epsilon_1 < 0$, then the edge force F_e and corresponding bolt stress σ have to be determined to satisfy the edge condition of zero penetration (i.e., $\epsilon_1 = 0$). The method to obtain this is described in Step II.

Step II. As determined in the foregoing, the bolt stress σ corresponds to edge gap ϵ_1. The edge gap ϵ_1 is an implicit function of σ and edge force, F_e, i.e.,

$$\epsilon_1 = f(\sigma, F_e) \tag{49}$$

Hence,

$$\epsilon_1 + \Delta\epsilon_1 = f + \left.\frac{\partial f}{\partial \sigma}\right|_{\sigma} \Delta\sigma + \left.\frac{\partial f}{\partial F_e}\right|_{F_e=0} \Delta F_e$$

Since $\epsilon_1 = f$ and we aim to set $\epsilon_1 + \Delta\epsilon_1 = 0$, we have

$$\left.\frac{\partial f}{\partial \sigma}\right|_{\sigma} \Delta\sigma + \left.\frac{\partial f}{\partial F_e}\right|_{F_e=0} \Delta F_e = -\epsilon_1 \tag{49a}$$

Similarly, the computed bolt length ℓ is an implicit function of σ and F_e (via equation (42) and (43)). Hence

$$\ell = g(\sigma, F_e) \tag{50}$$

The bolt length ℓ_b corresponding to bolt stress σ is

$$\ell_b = \frac{(\sigma - \sigma_0)\ell_0}{E_b} + \ell_0 \tag{50a}$$

Hence,

$$\tau = \ell - \ell_b = g(\sigma, F_e) - \ell_0 - \frac{(\sigma - \sigma_0)\ell_0}{E_b} \tag{51}$$

Thus the increments in σ and F_e required to make τ zero are given by

$$-\tau = \left(\frac{\partial g}{\partial \sigma} - \frac{\ell_0}{E_b}\right)\Delta\sigma + \left.\frac{\partial g}{\partial F_e}\right|_{F_e=0} \Delta F_e \tag{51a}$$

Equations (49a) and (51a) are solved for $\Delta\sigma$, and ΔF_e. Then the corrected value of σ and F_e are

$$\sigma_c = \sigma + \Delta\sigma$$

$$F_e = \Delta F_e \tag{51b}$$

If ϵ_1 and τ are zero (within a specified tolerance) corresponding to the corrected values of bolt stress and edge load, then the convergence is achieved. Otherwise, this process is repeated, until the convergence is obtained. The rate of convergence depends on the nonlinearity of the gasket stress-strain curve. Convergence was obtained in 1 to 3 iterations in the cases investigated by this author.

6 Closure

A comprehensive solution procedure to determine the stress and displacement fields in a three element flanged joint has been developed. The method described herein can be effectively employed to design flanged joints with precision, to maintain a predetermined residual bearing pressure on the gasket surface under the pressurized condition. The concept of controlled Metal-to-Metal contact on mating flange tips has also been introduced. In a sequel to this paper [16], this analysis technique is further utilized to evaluate the influence of the joint displacement fields on the thermal performance of the heat exchangers. In addition, numerical study of a typical joint is performed in that paper to demonstrate how "controlled" MTM can be exploited to achieve certain design goals.

References

1 "Pressure Vessel and Piping Design, Collected Papers 1927–1959," ASME, New York, 1960.

2 Waters, E. O., Wesstrom, D. B., Rossheim, D. B., and Williams, F. S. G., "Formulas for Stresses in Bolted Flanged Connections," TRANS. ASME, Vol. 59, 1937, pp. 161–169.

3 "ASME Boiler and Pressure Vessel Code, Section III. Subsection NA," ASME, New York, 1974 (including up to summer 75 addenda).

4 *"Standards of Tubular Manufacturer's Association,"* Fifth ed., TEMA, New York, 1968.

5 Soler, A. I., and Soehrens, J., "Stress Analysis of a U-Tube Heat Exchanger Tubesheet With Integral Channel, Head and Unperforated Rim," Joint Petroleum Mechanical Engineering and Pressure Vessels and Piping Conference, Mexico City, Mex., 1976, Paper No. 76-PVP-58, Sept. 19–24.

6 Gardner, K. A., "Heat Exchanger Tubesheet Design—3. U Tube and Bayonet Tubesheets," *Journal of Applied Mechanics*, Vol. 27, TRANS. ASME, Vol. 82, 1960, pp. 25–32.

7 Stevens-Guille, P. D., and Crago, W. A., "Application of Spiral Wound Gaskets for Leak-Tight Joints," *Journal of Pressure Vessel Technology*, TRANS. ASME, Series J, Vol. 97, No. 1, Feb. 1975, pp. 29–33; see also Discussion by K. P. Singh, *Journal of Pressure Vessel Technology*, TRANS. ASME, Series J, Vol. 98, No. 1, Feb. 1976, pp. 81–83.

8 Slot, T., and O'Donnel, W. J., "Effective Elastic Constants for Thick Perforated Plates With Square and Triangular Penetration Patterns," *Pressure Vessel and Piping: Design and Analysis*, Vol. 2, ASME, 1972, pp. 1081–1101.

9 Sampson, R. C., "Photoelastic Analysis of Stresses in Perforated Material Subject to Tension or Bending," *Bettis Technical Review*, WAPD-BT-18, Apr. 1960.

10 Soler, A. I., and Hill, W. S., "Effective Bending Properties for Stress Analysis of Rectangular Tubesheets," Paper No. 76-WA/Pwr-1, *Journal of Engineering for Power*, TRANS. ASME, Series A, Vol. 99, No. 3, 1977, pp. 365–370.

11 Timoshenko, S. P., and Woinowski-Krieger, S., *Theory of Plates and Shells*, McGraw-Hill, New York, Chapter 3, 1959, pp. 51–57.

12 Murray, N. W., and Stuart, D. G., "Behaviour of Large Taper Hub Flanges," *Proceedings of the Symposium Pressure Vessel Research Toward Better Design*, I. Mech. E., 1961, p. 133.

13 Rose, R. T., "Flanges", Chapter 6, *The Stress Analysis of Pressure Vessels and Pressure Vessel Components*, S. S. Gill, ed., Pergamon Press, 1970, pp. 267–315.

14 Hildebrand, F. B., *Advanced Calculus for Applications*, Prentice Hall, 1962, pp. 156–159.

15 Caranahan, B., Luther, H. A., Wilkes, D. O., *Applied Numerical Methods*, Wiley, New York, 1969, pp. 71–75.

16 Singh, K. P., "Study of Bolted Joint Integrity and Inter-Tube-Pass Leakage in U-Tube Heat Exchangers; Part II: Applications," ASME JOURNAL OF ENGINEERING FOR POWER, Vol 101, No. 1, pp. 16–22.

APPENDIX

Schleicher Functions

The Schleicher functions used in Section 4 are directly related to Ber and Bei functions [15]. In the interest of completeness, their series expansions are given below

$$\psi_1(x) = ber(x) = \sum_{k=0}^{\infty} (-1)^k \frac{z^{4k}}{[(2k)!]^2}$$

where $z = 0.5x$

$$\psi_2(x) = -bei(x) = \sum (-1)^{k+1} \frac{z^{4k+2}}{[(2k+1)!]^2}$$

$$\psi_3(x) = 0.5\psi_1(x) - \frac{2}{\pi}[R_1(x) + \psi_2(x) \cdot \ell n\, \beta z]$$

where $\beta = 1.78108$ and

$$R_1(x) = \sum_{k=0}^{\infty} (-1)^k \frac{S'_{2k+1}}{[(2k+1)!]^2} \cdot z^{4k+2}$$

$$S'_n = \sum_{j=1}^{n} \frac{1}{j}$$

$$\psi_4(x) = 0.5\psi_2(x) + \frac{2}{\pi}[R_2(x) + \psi_1(x) \cdot \ell n\, \beta z]$$

where

$$R_2 = \sum_{k=0}^{\infty} (-1)^k \frac{(2k+2)S'_{2k+2}}{[(2k+2)!]^2} z^{4k+3}$$

Finally the S-functions are defined as follows:

$$S_1(x) = x\psi_2(x) - 2\psi_1'(x)$$

$$S_2(x) = x\psi_1(x) + 2\psi_2'(x)$$

$$S_3(x) = x\psi_4(x) - 2\psi_3'(x)$$

$$S_4(x) = x\psi_3(x) + 2\psi_4'(x)$$

$$S_5(x) = x^2\psi_2'(x) - 4x\psi_2(x) + 8\psi_1'(x)$$

$$S_6(x) = x^2\psi_1'(x) - 4x\psi_1(x) - 8\psi_2'(x)$$

$$S_7(x) = x^2\psi_4'(x) - 4x\psi_4(x) + 8\psi_3'(x)$$

$$S_8(x) = x^2\psi_3'(x) - 4x\psi_3(x) - 8\psi_4'(x)$$

For small values of x, the series for Schleicher functions converge rapidly. For large values ($x \geq 6$), asymptotic approximations given in reference [12, p. 496] are sufficiently accurate.